INTERNATIONAL JOURNAL OF
NUMERICAL ANALYSIS AND MODELING
Volume 15, Number 1-2, Pages 134–153

AN ASYMPTOTIC PRESERVING IMPLICIT UNIFIED GAS KINETIC SCHEME FOR FREQUENCY-DEPENDENT RADIATIVE TRANSFER EQUATIONS

WENJUN SUN, SONG JIANG, AND KUN XU

Abstract. In this paper, an asymptotic preserving implicit unified gas kinetic scheme (IUGKS) is constructed for the frequency-dependent radiative transfer equations. Different from the asymptotic preserving unified gas kinetic scheme (UGKS) which uses the explicit initial value of the radiation intensity in the construction of the boundary fluxes as in the previous works [Sun et al., J. Comput. Phys. 285 (2015), pp. 265-279 and J. Comput. Phys. 302 (2015), pp. 222-238], here we construct the boundary fluxes by a back-time discretization so that they depend implicitly on the radiation intensity. Thus, the time step constraint by the Courant-Friedrichs-Lewy (CFL) condition is not needed anymore for IUGKS. It is shown that IUGKS is asymptotic preserving uniformly with the small Knudsen parameter. A number of numerical tests have been carried out and the numerical results show that large time steps can be used for the current scheme, and the computational efficiency can be improved greatly in comparison with UGKS and the implicit Monte Carlo scheme.

Key words. radiative transfer, frequency-dependent, asymptotic preserving, implicit unified gas kinetic scheme(IUGKS).

1. Introduction

Numerical solution of the radiative transfer equations is very important in many research fields, such as in astrophysics, inertial confinement fusion, and high temperature flow systems. Due to the complexity and higher dimensionality of the system, the numerical solution of the radiative transfer equations is very challenging, and its study attracts continuous attention from national laboratories and academic institutes. In this paper we shall make a continuous effort to develop a useful and reliable computational method for multiple scale radiative transfer systems.

The radiative transfer equations are the modeling equations in the kinetic level, where the photon transport and collision with material are taken into account. This system can present different limiting solutions with the changing of the scales. For the gray radiative transfer equations, the opacity is just a function of the material temperature. Therefore, the spatial cells can be classified as optical thick and optical thin regions, and a domain decomposition method with different numerical discretization in different regions can be developed. However, for the frequency-dependent radiative transfer equations, the opacity is typically a decreasing function of frequency. A spatial region can be optically thick for low frequency photon, but optically thin for high frequency ones.

Since the radiative transfer equations model the radiation intensity transport and energy exchange with the background material. The properties of the background material influence greatly on the behavior of radiation transfer. For a low opacity (background) material, the interaction between the radiation and material is weak, and the radiation propagates in a transparent way. The numerical method in this regime can be well developed by tracking the particle streaming transport.

Received by the editors March 5, 2017 and, in revised form, April 15, 2017.
2000 *Mathematics Subject Classification.* 85A25, 85-08, 65M99.

However, for a high opacity (background) material, there is severe interaction between radiation and material with a diminishing photon mean free path. As a result, the diffusive radiative behavior will dominate. In order to solve the kinetic scale based radiative transfer equations numerically, a straightforward way is to use a spatial mesh size which is comparable with photon's mean-free path, i.e., the so-called optical thin cell, and the transport equation can be discretized directly, such as using upwind approach for photon transport. This kind of method is basically a single scale method, where the numerical resolution down to the mean free path is used everywhere in the computation. Most Monte Carlo methods for transport equations belong to this category as well. In this kind of methods, to take such a small cell size will be associated with huge computational costs in the optical thick regime. In order to use a large cell size in comparison with the mean free path in the optical thick region, instead of decoupling the particle transport and collision in the numerical discretization, the coupled transport and collision has to be taken into account in the design of the scheme.

One of the efficient multiscale methods is to develop the so-called asymptotic preserving (AP) scheme for the kinetic equation. When holding the mesh size and time step fixed and as the Knudsen number going to zero, the AP scheme should automatically recover the discrete diffusion solution. AP schemes were first studied in the numerical solution of steady neutron transport problems by Larsen, Morel and Miller [17], Larsen and Morel [16], and then by Jin and Levermore [10,11], and the others. For unsteady problems, one of the AP schemes was constructed based on a decomposition of the distribution function between an equilibrium part and its non-equilibrium derivation, see Klar [13,14], and Jin, Pareschi and Toscani [12] for details. The development of an AP-type discrete ordinate method (DOM) for the multi-frequency radiative transfer equation coupled with material energy equation is a challenging numerical problem [8, 21], where most well-validated approaches are the Monte Carlo methods.

The unified gas kinetic scheme (UGKS) is one of the AP schemes for the transport equations [9, 22, 24, 26, 27]. It not only recovers accurate limiting solutions, such as ballistic transport and diffusion propagation, but also presents reliable solution in the whole transition regime. In UGKS, the mesh size is used directly as a modeling scale for identifying transport dynamics. When the mesh size is on the order of mean free path, the kinetic transport mechanism, such as the modeling process of the Boltzmann equation, is recovered in the numerical evolution [25]. When the mesh size is much larger than the mean free path, the hydrodynamic scale physics, such as the Navier-Stokes (NS) solutions for the flow system and the diffusion equation for the radiative transfer, is obtained. Between these two limits, a smooth transition is constructed and used for the capturing of non-equilibrium phenomena. In UGKS the mesh size and time step are dynamic variables in the evolution model. It may not be difficult to accept this kind of concept if we can realize that all fluid dynamic equations, such as the Boltzmann equation and the NS equations, are constructed based on their specific modeling scales with the corresponding dynamics.

In the previous works, we have developed an asymptotic preserving UGKS for the gray radiative transfer equations [22], and then an extension to frequency-dependent radiative transfer system [27]. Because the reconstruction method for the boundary fluxes in ([22], [27]) is explicit with the initial value of the radiative intensity, the time step should be constrained by the Courant-Friedrichs-Lewy (CFL) condition. The computational times could be very large for small spatial

meshes since the time step is small. And on the other hand, for the usual radiation hydrodynamics codes which solve the coupled equations of radiation with hydrodynamics, in order to save the computational time, the time step is usually constrained only by the hydrodynamical part, that is to say, the numerical method for the radiation equation should be stable for the large time step.

In this paper, by implicitly constructing the boundary fluxes with the radiative intensity, we propose an implicit asympotic preserving unified gas kinetic scheme (AP-IUGKS) for the frequency-dependent radiative transfer equations, which are composed of the radiation transport and material energy equations, and much more complicated in terms of dynamic modeling.

The basic steps in the construction of AP-IUGKS are the following. The multi-group method is first used to discretize the frequency variable, and the discrete-ordinate method (DOM) is employed to discretize the angular distribution of photon's movement. A time evolution integral solution of radiation intensity at different frequency is constructed for the flux evaluation at a cell interface. In order to evaluate the source terms inside each cell for the radiation intensity update, the macroscopic radiation energy equations at each frequency and the material energy equation are solved first at the next time level for the update of the macroscopic radiation energy and material temperature. Then, the updated macroscopic quantities are used in IUGKS for the full determination of the multi-group radiation intensity inside the cell. For the current AP-IUGKS, the large time step can be used in small spatial meshes, computational costs can be saved therefore, and the asymptotic preserving property of AP-IUGKS holds uniformly with respect to the small Knudsen number. For the multiple frequency radiative transfer, much numerical work is involved in the numerical discretization in the radiation frequency space and their coupling. Also, due to the complicated nature of such a system, we can only find the numerical examples, which have been previously tested by the Monte Carlo methods. We could not find any other DOM for the multiple frequency radiative transfer system [8, 21].

This paper is organized as follows. Section 2 introduces the model of the frequency-dependent radiative transfer equations. Section 3 is devoted to the construction of the implicit unified gas kinetic scheme (IUGKS). In Section 4 we show the asymptotic preserving property of IUGKS. In Section 5 a number of frequency-dependent numerical radiative transfer tests are included to demonstrate the accuracy and robustness of the new scheme, and its computational efficiency in comparison with the explicit unified gas kinetic scheme and implicit Monte Carlo method (IMC). A conclusion is given in the last section.

2. System of the radiative transfer equations

The gray and the frequency-dependent radiative transfer equations describe the radiative transfer and the energy exchange between radiation and materials. For the frequency-dependent case, the system can be written in following scaled form:

$$\begin{cases} \dfrac{\epsilon^2}{c}\dfrac{\partial I}{\partial t} + \epsilon\vec{\Omega}\cdot\nabla I = \sigma(B(\nu,T) - I), \\ \epsilon^2 C_v \dfrac{\partial T}{\partial t} \equiv \epsilon^2 \dfrac{\partial U}{\partial t} = \displaystyle\int_{4\pi}\int_0^\infty \sigma\Big(I - B(\nu,T)\Big) d\nu d\vec{\Omega}. \end{cases} \tag{1}$$

Here $I(t,\vec{r},\vec{\Omega},\nu)$ is the radiation intensity, $\vec{r}$ is the spatial variable, $\vec{\Omega}$ is the angular variable, t is the time, and $\nu \in (0,+\infty)$ is the frequency variable. $T(\vec{r},t)$ is the material temperature, $\sigma(\vec{r},\nu,T)$ is the opacity, c is the speed of light, $\epsilon > 0$ is the

Knudsen number, and $U(\vec{r},t)$ is the material energy density. For the simplicity of presentation, we have omitted the internal source and scattering terms in (1). In addition, the Planck function $B(\nu,T)$ is defined by

$$B(\nu,T)=\frac{2h\nu^3}{c^2}\frac{1}{e^{h\nu/kT}-1}, \tag{2}$$

where h is Planck's constant and k is Boltzmann's constant.

The material temperature $T(\vec{r},t)$ and the material energy density $U(\vec{r},t)$ are related by

$$\frac{\partial U}{\partial T}=C_{_V}>0,$$

where $C_{_V}(\vec{r},t)$ is the heat capacity.

As the parameter $\epsilon\to 0$, Larsen et al. [18] have shown that for frequency-dependent radiative transfer equation (1), away from boundaries and initial times, the intensity I approaches to a Planckian at the local temperature, i.e.,

$$I^{(0)}=B(\nu,T^{(0)}),$$

and the corresponding local temperature $T^{(0)}$ satisfies the following nonlinear diffusion equation,

$$\frac{\partial}{\partial t}U(T^{(0)})+a\frac{\partial}{\partial t}(T^{(0)})^4=\nabla\cdot\frac{ac}{3\sigma_R}\nabla(T^{(0)})^4, \tag{3}$$

where a is the radiation constant given by

$$a=\frac{8\pi k^4}{15h^3c^3},$$

and σ_R is the Rosseland mean opacity defined by

$$\frac{1}{\sigma_R}=\frac{\int_0^\infty\frac{1}{\sigma(\vec{r},\nu,T)}\frac{\partial B(\nu,T)}{\partial T}d\nu}{\int_0^\infty\frac{\partial B(\nu,T)}{\partial T}d\nu}.$$

An asymptotic preserving (AP) scheme for the frequency-dependent radiative transfer equations (1) is a numerical scheme which discretizes (1) in such a way that it leads to a correct discretization of the diffusion limit (3) when ϵ is small, and the scheme should be uniformly stable in the parameter ϵ.

The limiting equation (3) is what we would like to get in the AP scheme for (1) in the optical thick region. In the following, for the simplicity of presentation of our IUGKS method, we consider here the two-dimensional Cartesian spatial case for problem (1). Thus in this case, the angle direction is denoted by $\vec{\Omega}=(\mu,\xi)$, with $\mu=\sqrt{1-\zeta^2}\cos\theta$, $\xi=\sqrt{1-\zeta^2}\sin\theta$, $\zeta\in[-1,1]$ as the cosine value of the angle between the propagation direction $\vec{\Omega}$ and the z-axis, and $\theta\in[0,2\pi)$ as the angle between the projection vector of $\vec{\Omega}$ onto the xy-plane and the x-axis. Due to the symmetry of angular distribution in the two dimensional Cartesian case, we need consider $\zeta\geq 0$ only.

3. An IUGKS for the radiative transfer equations

In this section, based on the UGKS framework in [9,20,22,26,27], we will present firstly the AP-IUGKS for the frequency-dependent radiative transfer system (1).

3.1. Frequency space discretization for the system (1). The discretization of the frequency variable for the system (1) is similar to that in [27], here for completeness, we give the discretization of frequency variable ν in this subsection. A standard way is to apply a multi-group method in which the frequency variable ν is divided into discrete frequency intervals and the photons are "grouped" according to these intervals [1]. Let G be a positive integer number, we discretize the continuous frequency space $(0,+\infty)$ by G discrete frequency intervals $(\nu_{g-\frac{1}{2}},\nu_{g+\frac{1}{2}})$ with $g=1,\cdots,G$, and $\nu_{\frac{1}{2}}=0,\nu_{G+\frac{1}{2}}=+\infty$. Once the boundaries of the groups are defined, we can integrate the first equation in (1) over the frequency interval to get

$$\int_{\nu_{g-\frac{1}{2}}}^{\nu_{g+\frac{1}{2}}}(\frac{\epsilon}{c}\partial_t I+\vec{\Omega}\cdot\nabla I)d\nu=\int_{\nu_{g-\frac{1}{2}}}^{\nu_{g+\frac{1}{2}}}\frac{\sigma}{\epsilon}(B(\nu,T)-I)d\nu. \tag{4}$$

For the equation (4), the radiation intensity in different groups and the corresponding group opacities are given by

$$I_g=\int_{\nu_{g-\frac{1}{2}}}^{\nu_{g+\frac{1}{2}}}I(t,\vec{r},\vec{\Omega},\nu)d\nu, \tag{5}$$

and

$$\sigma_g^e=\frac{\displaystyle\int_{\nu_{g-\frac{1}{2}}}^{\nu_{g+\frac{1}{2}}}\sigma B(\nu,T)d\nu}{\displaystyle\int_{\nu_{g-\frac{1}{2}}}^{\nu_{g+\frac{1}{2}}}B(\nu,T)d\nu},\qquad \sigma_g^a=\frac{\displaystyle\int_{\nu_{g-\frac{1}{2}}}^{\nu_{g+\frac{1}{2}}}\sigma I d\nu}{\displaystyle\int_{\nu_{g-\frac{1}{2}}}^{\nu_{g+\frac{1}{2}}}I d\nu}. \tag{6}$$

We also integrate the Planck function $B(\nu,T)$ on the right hand side of (4) over the frequency interval, and denote

$$\phi_g=\int_{\nu_{g-\frac{1}{2}}}^{\nu_{g+\frac{1}{2}}}B(\nu,T)d\nu. \tag{7}$$

With these notations in (5)–(7), the equations (1) are reduced to a multi-group radiative transfer system:

$$\begin{cases}\dfrac{\epsilon^2}{c}\dfrac{\partial I_g}{\partial t}+\epsilon\vec{\Omega}\cdot\nabla I_g=(\sigma_g^e\phi_g-\sigma_g^a I_g),\quad (g=1,\cdots,G),\\ \epsilon^2 C_v\dfrac{\partial T}{\partial t}\equiv\epsilon^2\dfrac{\partial U}{\partial t}=\displaystyle\sum_{g=1}^{g=G}\int_{4\pi}(\sigma_g^a I_g-\sigma_g^e\phi_g)d\vec{\Omega}.\end{cases} \tag{8}$$

It should be noted that the absorption opacity σ_g^a which is a weighted integration with the unknown function I. Usually, the unknown function I in this opacity integration is replaced by the Planck function with the radiation temperature T_r instead of the material temperature T. For this purpose, we define the radiation temperature and the absorption opacity in the following way,

$$acT_r^4=\int_{4\pi}\int_0^{+\infty}Id\vec{\Omega}d\nu=\sum_{g=1}^{g=G}\int_{4\pi}I_g d\vec{\Omega},\qquad \sigma_g^a=\frac{\displaystyle\int_{\nu_{g-\frac{1}{2}}}^{\nu_{g+\frac{1}{2}}}\sigma B(\nu,T_r)d\nu}{\displaystyle\int_{\nu_{g-\frac{1}{2}}}^{\nu_{g+\frac{1}{2}}}B(\nu,T_r)d\nu}. \tag{9}$$

Up to now, the discretization of the frequency variable is finished.

3.2. Angular, spatial and time discretizations of the system (8). First, for the angular variable of the system (8), as done for the usual discrete ordinate method, we give the propagation direction (μ, ξ) a set of discrete values. As in [19] for example, we use an even integer N as the discrete ordinate order, then obtain the discrete directions $\vec{\Omega}_m = (\mu_m, \xi_m)$ and their corresponding integration weights ω_m for $m = 1, \cdots, M$, with $M = N(N+2)/2$. For each direction (μ_m, ξ_m), we get the following discrete equations for the system (8):

(10)
$$\begin{cases} \dfrac{\epsilon^2}{c}\dfrac{\partial I_{m,g}}{\partial t} + \epsilon\vec{\Omega}_m \cdot \nabla I_{m,g} = (\sigma_g^e \phi_g - \sigma_g^a I_{m,g}), \quad (g = 1, \cdots, G, \quad m = 1, \cdots, M), \\ \epsilon^2 C_v \dfrac{\partial T}{\partial t} \equiv \epsilon^2 \dfrac{\partial U}{\partial t} = \displaystyle\sum_{g=1}^{g=G}\sum_{m=1}^{m=M} (\sigma_g^a I_{m,g} - \sigma_g^e \phi_g)\omega_m. \end{cases}$$

As for the spatial and time variables, let $x_i = i\Delta x$, $y_j = j\Delta y$ and $t^n = n\Delta t$ $(i, j, n \in \mathbb{Z})$ be the uniform mesh in Cartesian coordinates, where $\Delta x, \Delta y$ and Δt are the mesh sizes in the x-, y-directions and the time step in the t-direction. Let (i, j) denote the cell $\{(x, y);\ x_{i-1/2} < x < x_{i+1/2}, y_{j-1/2} < y < y_{j+1/2}\}$, where $x_{i-1/2} = (i - \frac{1}{2})\Delta x$ and $y_{j-1/2} = (j - \frac{1}{2})\Delta y$ are the cell interfaces.

In what follows, we denote by $I^n_{i,j,m,g}$ the cell averaged value of the intensity $I_{m,g}$ at time t^n in cell (i, j) with cell center (x_i, y_j). Then, we integrate the equations (10) over the cell (i, j) from time t^n to $t^n + \Delta t$. A conservative finite volume numerical scheme for the equations (10) is of the form

(11)
$$\begin{cases} I^{n+1}_{i,j,m,g} = I^n_{i,j,m,g} + \frac{\Delta t}{\Delta x}(F^{n+1}_{i-1/2,j,m,g} - F^{n+1}_{i+1/2,j,m,g}) \\ \qquad\qquad + \frac{\Delta t}{\Delta y}(H^{n+1}_{i,j-1/2,m,g} - H^{n+1}_{i,j+1/2,m,g}) + \frac{c\Delta t}{\epsilon^2}\{(\sigma_g^e \tilde{\phi}_{g,i,j} - \sigma_g^a \tilde{I}_{i,j,m,g})\}, \\ \epsilon^2 C_v T^{n+1}_{i,j} = \epsilon^2 C_v T^n_{i,j} + \Delta t \displaystyle\sum_{g=1}^{g=G}\sum_{m=1}^{m=M} (\sigma_g^a \tilde{I}_{i,j,m,g} - \sigma_g^e \tilde{\phi}_{g,i,j})\omega_m, \end{cases}$$

where $F^{n+1}_{i-1/2,j,m,g}$ and $H^{n+1}_{i,j-1/2,m,g}$ are the time-dependent numerical fluxes in the x- and y-directions across the cell interfaces which are implicitly depending on the values of $I^{n+1}_{i,j,m,g}$; and the terms on the right hand side of (11) are given by

(12)
$$\begin{aligned} F^{n+1}_{i-1/2,j,m,g} &= \frac{c}{\epsilon\Delta t}\int_{t^n}^{t^{n+1}} \mu_m I_{m,g}(t, x_{i-\frac{1}{2}}, y_j, \mu_m, \xi_m)dt, \\ H^{n+1}_{i,j-1/2,m,g} &= \frac{c}{\epsilon\Delta t}\int_{t^n}^{t^{n+1}} \xi_m I_{m,g}(t, x_i, y_{j-\frac{1}{2}}, \mu_m, \xi_m)dt, \\ \tilde{\phi}_{g,i,j} &= \frac{1}{\Delta t\Delta x\Delta y}\int_{t^n}^{t^{n+1}}\int_{x_{i-1/2}}^{x_{i+1/2}}\int_{y_{j-1/2}}^{y_{j+1/2}} \phi_g(t, x, y)dxdydt, \\ \tilde{I}_{i,j,m,g} &= \frac{1}{\Delta x\Delta y\Delta t}\int_{t^n}^{t^{n+1}}\int_{x_{i-1/2}}^{x_{i+1/2}}\int_{y_{j-1/2}}^{y_{j+1/2}} I_{m,g}(t, x, y, \mu_m, \xi_m)dxdydt. \end{aligned}$$

In order to update the system (11), we have to give all terms in (12) explicitly. First, the term $\tilde{I}_{i,j,m,g}$ in (12) can be approximated implicitly by

$$\tilde{I}_{i,j,m,g} \approx I^{n+1}_{i,j,m,g},$$

which can be incorporated into the left hand side of (11).

3.3. IUGKS: construction of the boundary fluxes. The key for IUGKS is to model the time-dependent interface fluxes $F^{n+1}_{i-1/2,j,m,g}$ and $H^{n+1}_{i,j-1/2,m,g}$ in (12) implicitly depending on the radiative intensity values of $I^{n+1}_{i,j,m,g}$. Different from the

explicit method used in [20, 22, 26] where the radiation intensity at a cell interface for building the boundary fluxes is based on an evolution solution of the transport equation with initial value $I^n_{i,j,m,g}$, in this paper we reconstruct the radiation intensity at a cell interface in boundary fluxes based on the value $I^{n+1}_{i,j,m,g}$. Thus, an implicit unified gas kinetic scheme for (11) is obtained. This evolution solution covers different flow regimes from the ballistic transport to the hydrodynamic wave propagation [24]. The real solution used for the flux evaluation depends on the ratio of the time step to the local particle collision time.

For the x-direction flux $F^{n+1}_{i-1/2,j,m,g}$, the radiation intensity on the interface is obtained by solving the following initial value problem at the cell boundary $x = x_{i-1/2}, y = y_j$:

$$\begin{cases} \frac{\epsilon}{c}\partial_t I_{m,g} + \mu_m \partial_x I_{m,g} = \frac{1}{\epsilon}(\sigma^e_g \phi_g - \sigma^a_g I_{m,g}), \\ I_{m,g}(x, y_j, t)|_{t=t^n} = \tilde{I}_{m,g,0}(x, y_j), \end{cases} \tag{13}$$

where the expressions of the initial value $\tilde{I}_{m,g,0}(x, y_j)$ and ϕ_g will be given later in details. Thus, a time dependent evolution solution can be obtained,

$$\begin{aligned} I_{m,g}(t, x_{i-1/2}, y_j, \mu_m, \xi_m) = {} & e^{-\lambda_{g,i-1/2,j}(t-t^n)} \tilde{I}_{m,g,0}(x_{i-1/2} - \tfrac{c\mu_m}{\epsilon}(t-t^n)) \\ & + \int_{t^n}^t e^{-\lambda_{g,i-1/2,j}(t-s)} \tfrac{c\sigma^e_{g,i-1/2,j}}{\epsilon^2} \phi_g(s, x_{i-1/2} - \tfrac{c\mu_m}{\epsilon}(t-s)) ds, \end{aligned} \tag{14}$$

where $\lambda_g = c\sigma^a_g/\epsilon^2$, and $\lambda_{g,i-1/2,j}$ denotes the value of λ_g at the corresponding cell boundary. Substituting $I_{m,g}(t, x_{i-1/2}, y_j, \mu_m, \xi_m)$ in (14) into $(12)_1$, and integrating the resulting identity with respect to time t from t^n to t^{n+1}, we can get the numerical flux $F^{n+1}_{i-1/2,j,m,g}$ in the x-direction. The numerical flux $H^{n+1}_{i,j-1/2,m,g}$ in the y-direction can be constructed similarly.

The solution in (14) depends on two functions, which need to be evaluated numerically. The first one is the value of $I_{m,g}(x, y_j, t)$ at t^n around $(x_{i-1/2}, y_j)$, i.e., the initial data $\tilde{I}_{m,g,0}(x, y_j)$, and the another is the value of the function $\phi_g(t, x, y)$ between the time steps t^n and t^{n+1} around the cell boundary $(x_{i-1/2}, y_j)$.

The initial data $\tilde{I}_{m,g,0}(x, y_j)$ at the beginning of each time step in (13) can be approximated by a piecewise linear function:

$$\tilde{I}_{m,g,0}(x, y_j) = \begin{cases} I^{n+1}_{i-1,j,m,g} + \delta_x I^n_{i-1,j,m,g}(x - x_{i-1}), & \text{if } x < x_{i-1/2}, \\ I^{n+1}_{i,j,m,g} + \delta_x I^n_{i,j,m,g}(x - x_i), & \text{if } x > x_{i-1/2}, \end{cases} \tag{15}$$

where $\delta_x I^n_{i-1,j,m,g}$, $\delta_x I^n_{i+1,j,m,g}$ are the reconstructed slopes through the second order MUSCL limiter [23] with initial date of $I^n_{i,j,m,g}$.

The value of the function $\phi_g(x, y_j, t)$ between the time steps t^n and t^{n+1} around the cell boundary $(x_{i-1/2}, y_j)$ is approximated by a piecewise continuous polynomial as:

$$\phi_g(x, y_j, t) = \bar{\phi}^{n+1}_{g,i-1/2,j} + \begin{cases} \delta_x \bar{\phi}^{n+1,L}_{g,i-1/2,j}(x - x_{i-1/2}), & \text{if } x < x_{i-1/2}, \\ \delta_x \bar{\phi}^{n+1,R}_{g,i-1/2,j}(x - x_{i-1/2}), & \text{if } x > x_{i-1/2}, \end{cases} \tag{16}$$

where the left and right one-sided finite differences are given by

$$\delta_x \bar{\phi}^{n+1,L}_{g,i-1/2,j} = \frac{\bar{\phi}^{n+1}_{g,i-1/2,j} - \bar{\phi}^{n+1}_{g,i-1,j}}{\Delta x/2}, \qquad \delta_x \bar{\phi}^{n+1,R}_{g,i-1/2,j} = \frac{\bar{\phi}^{n+1}_{g,i,j} - \bar{\phi}^{n+1}_{g,i-1/2,j}}{\Delta x/2}.$$

The cell boundary value $\bar{\phi}^{n+1}_{g,i-1/2,j}$ and the cell center values $\bar{\phi}^{n+1}_{g,i,j}$ and $\bar{\phi}^{n+1}_{g,i-1,j}$ will be determined in the next subsection. Given the above constructions, the numerical flux

$$F^{n+1}_{i-1/2,j,m,g} = \frac{c\mu_m}{\epsilon \Delta t} \int_{t^n}^{t^{n+1}} I_{m,g}(t, x_{i-1/2}, y_j, \mu_m, \xi_m) dt$$

can be exactly computed by using the expressions (14), (15) and (16),

$$
\begin{aligned}
F^{n+1}_{i-1/2,j,m,g} &= A_{g,i-1/2,j}\mu_m(I^-_{i-1/2,j,m,g}1_{\mu_m>0} + I^+_{i-1/2,j,m,g}1_{\mu_m<0}) \\
&+C_{g,i-1/2,j}\mu_m\bar{\phi}^{n+1}_{g,i-1/2,j} \\
&+D_{g,i-1/2,j}(\mu_m^2\delta_x\bar{\phi}^{n+1,L}_{g,i-1/2,j}1_{\mu_m>0} + \mu_m^2\delta_x\bar{\phi}^{n+1,R}_{g,i-1/2,j}1_{\mu_m<0}) \\
&+B_{g,i-1/2,j}(\mu_m^2\delta_x I^n_{i-1,j,m,g}1_{\mu_m>0} + \mu_m^2\delta_x I^n_{i,j,m,g}1_{\mu_m<0}),
\end{aligned} \tag{17}
$$

where $I^-_{i-1/2,j,m,g}$ and $I^+_{i-1/2,j,m,g}$ are the values at boundary, given by

$$
\begin{aligned}
I^-_{i-1/2,j,m,g} &= I^{n+1}_{i-1,j,m,g} + \tfrac{\Delta x}{2}\delta_x I^n_{i-1,j,m,g}, \\
I^+_{i-1/2,j,m,g} &= I^{n+1}_{i,j,m,g} - \tfrac{\Delta x}{2}\delta_x I^n_{i,j,m,g}.
\end{aligned} \tag{18}
$$

The coefficients in (17) are

$$
\begin{aligned}
A_g &= \tfrac{c}{\epsilon\Delta t\lambda_g}(1-e^{-\lambda_g\Delta t}), \\
C_g &= \tfrac{c^2\sigma^e_g}{\Delta t\epsilon^3\lambda_g}(\Delta t - \tfrac{1}{\lambda_g}(1-e^{-\lambda_g\Delta t})), \\
D_g &= -\tfrac{c^3\sigma^e_g}{\Delta t\epsilon^4\lambda_g^2}(\Delta t(1+e^{-\lambda_g\Delta t}) - \tfrac{2}{\lambda_g}(1-e^{-\lambda_g\Delta t})), \\
B_g &= -\tfrac{c^2}{\epsilon^2\lambda_g^2\Delta t}(1-e^{-\lambda_g\Delta t} - \lambda_g\Delta t e^{-\lambda_g\Delta t}),
\end{aligned} \tag{19}
$$

with $\lambda_g = c\sigma^a_g/\epsilon^2$. With the expression (19), we have

$$
\begin{aligned}
A_{g,i-1/2,j} &= A_g(\Delta t, \epsilon, \lambda_{g,i-1/2,j}), \\
C_{g,i-1/2,j} &= C_g(\Delta t, \epsilon, \sigma^e_{g,i-1/2,j}, \lambda_{g,i-1/2,j}), \\
D_{g,i-1/2,j} &= D_g(\Delta t, \epsilon, \sigma^e_{g,i-1/2,j}, \lambda_{g,i-1/2,j}), \\
B_{g,i-1/2,j} &= B_g(\Delta t, \epsilon, \lambda_{g,i-1/2,j}).
\end{aligned} \tag{20}
$$

It should be emphasized here that even with the interface solution (14), in order to obtain a consistent limiting diffusive flux, the coefficients, such as $\sigma^e_{g,i-1/2,j}$ and $\lambda_{g,i-1/2,j}$ at a cell boundary, have to be properly defined by using the values from the two neighboring cells in the above expression (20).

The boundary flux $H^{n+1}_{i,j-\frac{1}{2},m,g}$ in the y-direction can be constructed in the same way. This completes the construction of the numerical boundary fluxes for the multi-group radiative transfer equations (11).

3.4. IUGKS: evaluation of the macroscopic quantities in boundary fluxes. To complete the construction of numerical scheme for (10), the detailed expressions $\tilde{\phi_g}$ in (11), and $\bar{\phi}^{n+1}_{g,i-1/2,j}$, $\bar{\phi}^{n+1}_{g,i,j}$, and $\bar{\phi}^{n+1}_{g,i-1,j}$ in (16), have to be given. Following the methodology of UGKS, these quantities will be evaluated through the following macroscopic equations. First, taking the angular integration of the first equation in (8), we obtain the following system for the macroscopic variables:

$$
\begin{cases}
\dfrac{\epsilon^2}{c}\dfrac{\partial\rho_g}{\partial t} + \epsilon\nabla\cdot < \vec{\Omega}I_g >= (4\pi\sigma^e_g\bar{\phi}_g - \sigma^a_g\rho_g), \quad (g=1,\cdots,G), \\
\epsilon^2 C_v\dfrac{\partial\tilde{T}}{\partial t} \equiv \epsilon^2\dfrac{\partial U}{\partial t} = \displaystyle\sum_{g=1}^{g=G}(\sigma^a_g\rho_g - 4\pi\sigma^e_g\bar{\phi}_g),
\end{cases} \tag{21}
$$

where $\rho_g = \int_{4\pi} I_g d\vec{\Omega}$ and $< \vec{\Omega}I_g >$ is the angular vector integration given by

$$
< \vec{\Omega}I_g >= \int_{4\pi}\vec{\Omega}I_g d\vec{\Omega}.
$$

Then, the macroscopic equations (21) are implicitly discretized as follows.

(22)
$$\begin{cases} \rho_{g,i,j}^{n+1} = \rho_{g,i,j}^{n} + \frac{\Delta t}{\Delta x}(\Phi_{g,i-1/2,j}^{n+1} - \Phi_{g,i+1/2,j}^{n+1}) + \frac{\Delta t}{\Delta y}(\Psi_{g,i,j-1/2}^{n+1} - \Psi_{g,i,j+1/2}^{n+1}) \\ \qquad\qquad + \frac{c\Delta t}{\epsilon^2}(4\pi(\sigma_g^e)_{i,j}^{n+1}\bar{\phi}_{g,i,j}^{n+1} - (\sigma_g^a)_{i,j}^{n+1}\rho_{g,i,j}^{n+1}), \quad (g = 1, \cdots, G) \\ \\ C_v\tilde{T}_{i,j}^{n+1} = C_v\tilde{T}_{i,j}^{n} + \frac{\Delta t}{\epsilon^2}\sum_{g=1}^{g=G}\big((\sigma_g^a)_{i,j}^{n+1}\rho_{g,i,j}^{n+1} - 4\pi(\sigma_g^e)_{i,j}^{n+1}\bar{\phi}_{g,i,j}^{n+1}\big), \end{cases}$$

where the cell interface fluxes are given by

$$\begin{array}{l} \tilde{T}_{i,j}^{n} = T_{i,j}^{n}, \quad \rho_{g,i,j}^{n} = \int_{4\pi} I_g^n d\vec{\Omega} \\ \Phi_{g,i-1/2,j}^{n+1} = \frac{c}{\epsilon\Delta t}\int_{t^n}^{t^n+\Delta t} < \Omega_x I_g > (x_{i-1/2}, y_j, t)dt, \\ \Phi_{g,i+1/2,j}^{n+1} = \frac{c}{\epsilon\Delta t}\int_{t^n}^{t^n+\Delta t} < \Omega_x I_g > (x_{i+1/2}, y_j, t)dt, \\ \Psi_{g,i,j-1/2}^{n+1} = \frac{c}{\epsilon\Delta t}\int_{t^n}^{t^n+\Delta t} < \Omega_y I_g > (x_i, y_{j-1/2}, t)dt, \\ \Psi_{g,i,j+1/2}^{n+1} = \frac{c}{\epsilon\Delta t}\int_{t^n}^{t^n+\Delta t} < \Omega_y I_g > (x_i, y_{j+1/2}, t)dt. \end{array} \tag{23}$$

With the help of the cell interface intensity I_g $(g = 1, \cdots, G)$ in (14), we can get an explicit expression for all terms in (23). For example, at the cell interface in the x-direction, we can have

(24)
$$\begin{aligned} \Phi_{g,i-1/2,j}^{n+1} &= \tfrac{c}{\epsilon\Delta t}\textstyle\int_{t^n}^{t^n+\Delta t} < \Omega_x I_g > (x_{i-1/2}, y_j, t)dt \\ &= \textstyle\sum_{m=1}^{M}\omega_m F_{i-1/2,j,m,g} \\ &= A_{g,i-1/2,j}^{n+1}\textstyle\sum_{m=1}^{M}\omega_m\mu_m(I_{i-1,j,m,g}^{-}1_{\mu_m>0} + I_{i,j,m,g}^{+}1_{\mu_m<0}) \\ &\quad + \frac{4\pi D_{g,i-1/2,j}^{n+1}}{3}\big(\frac{\bar{\phi}_{g,i,j}^{n+1} - \bar{\phi}_{g,i-1,j}^{n+1}}{\Delta x}\big) \\ &\quad + B_{g,i-1/2,j}^{n+1}\textstyle\sum_{m=1}^{M}\omega_m\mu_m^2(\delta_x I_{i-1,j,m,g}^{n}1_{\mu_m>0} + \delta_x I_{i,j,m,g}^{n}1_{\mu_m<0}), \end{aligned}$$

where the expressions of $A_{g,i-1/2,j}^{n+1}, B_{g,i-1/2,j}^{n+1}$ and $D_{g,i-1/2,j}^{n+1}$ in (24) are the same as those of the parameters $A_{g,i-1/2,j}$, $B_{g,i-1/2,j}$, and $D_{g,i-1/2,j}$ in (20), but with the following definitions for the cell interface values $(\sigma_g^a)_{i-1/2,j}$ and $(\sigma_g^e)_{i-1/2,j}$,

$$(\sigma_g^a)_{i-1/2,j}^{n+1} = \frac{2(\sigma_g^a)_{i,j}^{n+1}(\sigma_g^a)_{i-1,j}^{n+1}}{(\sigma_g^a)_{i,j}^{n+1} + (\sigma_g^a)_{i-1,j}^{n+1}}, \qquad (\sigma_g^e)_{i-1/2,j}^{n+1} = \frac{2(\sigma_g^e)_{i,j}^{n+1}(\sigma_g^e)_{i-1,j}^{n+1}}{(\sigma_g^e)_{i,j}^{n+1} + (\sigma_g^e)_{i-1,j}^{n+1}}. \tag{25}$$

Now, with the given interface fluxes in (23), the equations (22) become a coupled nonlinear system for the macroscopic quantities $\tilde{T}_{i,j}^{n+1}$ and $\rho_{g,i,j}^{n+1}$ $(g = 1, \cdots, G)$, where the parameters $(\sigma_g^a)_{i,j}^{n+1}$ and $(\sigma_g^e)_{i,j}^{n+1}$ depend implicitly on the material temperature $\tilde{T}_{i,j}^{n+1}$, and the macro boundary fluxes depend on the radiative intensity $I_{i,j,m,g}^{n+1}$ implicitly. This nonlinear system can be solved by employing an iterative method, and its solution procedure should be coupled with the solution of the multi-group radiative transfer equations (10), which will be described in details in the next subsection.

Once one obtains $\tilde{T}_{i,j}^{n+1}$ in the macroscopic variable equations (21), one can get $\bar{\phi}_{g,i,j}^{n+1}$ $(g = 1, \cdots, G)$ through (7) with the material temperature T being replaced by $\tilde{T}_{i,j}^{n+1}$. Then, $\tilde{\phi}_{g,i,j}$ in (12) can be linearized and is set by

$$\tilde{\phi}_{g,i,j} = \bar{\phi}_{g,i,j}^{n+1} + \frac{\partial\bar{\phi}_{g,i,j}}{\partial T}(T_{i,j}^{n+1} - \tilde{T}_{i,j}^{n+1}), \tag{26}$$

and the cell interface value $\bar{\phi}^{n+1}_{g,i-1/2,j}$ in (16) takes

$$\bar{\phi}^{n+1}_{g,i-1/2,j} = \frac{1}{2}(\bar{\phi}^{n+1}_{g,i-1,j} + \bar{\phi}^{n+1}_{g,i,j}), \quad (g = 1, \cdots, G). \tag{27}$$

The cell interface opacities $(\sigma^a_g)_{i-1/2,j}$ and $(\sigma^e_g)_{i-1/2,j}$ are determined by (25) with the above updated material temperature $\tilde{T}^{n+1}_{i,j}$ from the macro equations (21).

3.5. IUGKS: solution of the system (11). In the next subsection, we discretize the macroscopic equations (21) for the radiation energy $\rho^{n+1}_{g,i,j}$ and material temperature $\tilde{T}^{n+1}_{i,j}$. Different from the explicit method used in [22, 27], for the $I^{n+1}_{i,j,m,g}$-dependent macro boundary fluxes in (23), the macro quantities will be solved by interweaving with the solution of the radiative intensity equation (11). First, we assume these macro quantities are known, then the interface flux function for the radiation intensity of the system (12) is fully obtained although it implicitly depends on the values of the radiative intensity $I^{n+1}_{i,j,m,g}$. And the radiative transfer equations in (10) can be discretized as follows.

$$\begin{aligned} I^{n+1}_{i,j,m,g} = I^n_{i,j,m,g} &+ \tfrac{\Delta t}{\Delta x}(F^{n+1}_{i-1/2,j,m,g} - F^{n+1}_{i+1/2,j,m,g}) \\ &+ \tfrac{\Delta t}{\Delta y}(H^{n+1}_{i,j-1/2,m,g} - H^{n+1}_{i,j+1/2,m,g}) \\ &+ \tfrac{c\Delta t}{\epsilon^2}((\sigma^e_g)^{n+1}_{i,j}\tilde{\phi}_{g,i,j} - (\sigma^a_g)^{n+1}_{i,j} I^{n+1}_{i,j,m,g}), \end{aligned} \tag{28}$$

where the opacities $(\sigma^e_g)^{n+1}_{i,j}$ and $(\sigma^a_g)^{n+1}_{i,j}$ are fully determined by the updated material temperature $\tilde{T}^{n+1}_{i,j}$ of the macro equations (21), and the $\tilde{\phi}_{g,i,j}$ is given in (26).

The second equation of (10) for obtaining the final material temperature can be directly discretized by coupling with the value $I^{n+1}_{i,j,m,g}$, as follows.

$$C_v T^{n+1}_{i,j} = C_v T^n_{i,j} + \Delta t \sum_{g=1}^{g=G} \sum_{m=1}^{M} \omega_m((\sigma^a_g)^{n+1}_{i,j} I^{n+1}_{i,j,m,g} - (\sigma^e_g)^{n+1}_{i,j}\tilde{\phi}^{n+1}_{g,i,j})/\epsilon^2. \tag{29}$$

This completes the construction of AP-IUGKS for the frequency-dependent radiative transfer equations (1). Since these equations (28) and (29) are implicitly discretized and strongly coupled, they can be solved by using the source iteration method. We summarize the iteration steps of AP-IUGKS in the following.

Loop of AP-IUGKS: Given $I^n_{i,j,m,g}$ and $T^n_{i,j}$ at time step n, evaluate $\rho^n_{g,i,j}$ and $\phi^n_{g,i,j}$, and find $I^{n+1}_{i,j,m,g}$ and $T^{n+1}_{i,j}$ at time step $n+1$.

1) Let $T^{n+1,0}_{i,j} = T^n_{i,j}$ and $I^{n+1,0}_{i,j,m,g} = I^n_{i,j,m,g}$;
2) For $l = 1, 2, \cdots, L$,

2.1) Use $I^{n+1,l-1}_{i,j,m,g}$ to replace the implicit radiative intensity values $I^{n+1}_{i,j,m,g}$ in the macro-boundary fluxes of (23). Solve the system (22) to obtain $\tilde{T}^{n+1}_{i,j}$ and $\rho^{n+1}_{g,i,j}$, then $\bar{\phi}^{n+1}_{g,i,j}$;

2.2) Use the computed values $\tilde{T}^{n+1}_{i,j}$ and $\bar{\phi}^{n+1}_{g,i,j}$ from Step 2.1) to obtain the boundary fluxes $I^{n+1,l}_{i,j,m,g}$ in (28) by applying the source iteration method to implicitly solve (28).

2.3) Replace $I^{n+1}_{i,j,m,g}$ in (29) by $I^{n+1,l}_{i,j,m,g}$ to get the renewed value $T^{n+1,l}_{i,j}$ by using the explicit expression (29).

2.4) Compute the relative iteration error. Stop the iteration when the convergent requirement is satisfied.

3) Set $I^{n+1}_{i,j,m,g} = I^{n+1,l}_{i,j,m,g}, T^{n+1}_{i,j} = T^{n+1,l}_{i,j}$ and goto Step 1) for the next computational step.

In the above algorithm, the macro equation (22) and the radiative transfer equations (28) and (29) will be solved by iteration. Next, we describe the iteration methods used in the current scheme.

Iteration algorithm for solving (22)

Given $\rho^n_{g,i,j}$ and $\phi^n_{g,i,j}$ which are obtained based on the initial radiation intensity $I^n_{i,j,m,g}$ and $T^n_{i,j}$, find $\rho^{n+1}_{g,i,j}$, $\tilde{T}^{n+1}_{i,j}$ and $\bar{\phi}^{n+1}_{i,j,g}$ in the equations (22).

1) Set the initial iterative value: $\rho^{n+1,0}_{g,i,j} = \rho^n_{g,i,j}$ and $\tilde{T}^{n+1,0}_{i,j} = T^n_{i,j}$;

2) Calculate the value $\bar{\phi}^{n+1,0}_{g,i,j}$ by the formula (7) with $\tilde{T}^{n+1,0}_{i,j}$ in place of $T^n_{i,j}$;

3) For $s = 1, \cdots, S$,

3.1) Compute the coefficients $(\sigma^a_g)^{n+1,s}_{i,j}$, $(\sigma^e_g)^{n+1,s}_{i,j}$, $A^{n+1,s}_{g,i-1/2,j}$, $B^{n+1,s}_{g,i-1/2,j}$ and $D^{n+1,s}_{g,i-1/2,j}$, which are functions of $\tilde{T}^{n+1,s-1}_{i,j}$ and $I^{n+1,l}_{i-1,j,m,g}$, $I^{n+1,l}_{i,j,m,g}$, $I^{n+1,l}_{i+1,j,m,g}$.

3.2) Find $\rho^{n+1,s}_{g,i,j}$ and $\tilde{T}^{n+1,s}_{i,j}$ from the following iterative system:

$$
(30)\quad \begin{cases} \rho^{n+1,s}_{g,i,j} = \rho^n_{g,i,j} + \frac{\Delta t}{\Delta x}(\Phi^{n+1,s}_{g,i-1/2,j} - \Phi^{n+1,s}_{g,i+1/2,j}) + \frac{\Delta t}{\Delta y}(\Psi^{n+1,s}_{g,i,j-1/2} - \\ \qquad \Psi^{n+1,s}_{g,i,j+1/2}) + \frac{c\Delta t}{\epsilon^2}(4\pi(\sigma^e_g)^{n+1,s}_{i,j}\bar{\phi}^{n+1,s}_{g,i,j} - (\sigma^a_g)^{n+1,s}_{i,j}\rho^{n+1,s}_{g,i,j}), \\ C_v\tilde{T}^{n+1,s}_{i,j} = C_v T^n_{i,j} + \frac{\Delta t}{\epsilon^2}\sum_{g=1}^{G=G}((\sigma^a_g)^{n+1,s}_{i,j}\rho^{n+1,s}_{g,i,j} - 4\pi(\sigma^e_g)^{n+1,s}_{i,j}\bar{\phi}^{n+1,s}_{g,i,j}), \\ \bar{\phi}^{n+1,s}_{g,i,j} = \bar{\phi}^{n+1,s-1}_{g,i,j} + (\frac{\partial\bar{\phi}_g}{\partial T})^{n+1,s-1}_{i,j}(\tilde{T}^{n+1,s}_{i,j} - \tilde{T}^{n+1,s-1}_{i,j}), \\ (\frac{\partial\bar{\phi}_g}{\partial T})^{n+1,s-1}_{i,j} = (\int_{\nu_{g-\frac{1}{2}}}^{\nu_{g+\frac{1}{2}}} \frac{\partial B(\nu,T)}{\partial T}d\nu)|_{T=\tilde{T}^{n+1,s-1}_{i,j}}. \end{cases}
$$

Here $(\partial\bar{\phi}_g/\partial T)^{n+1,s-1}_{i,j}$ is a function of $\tilde{T}^{n+1,s-1}_{i,j}$, and the interface numerical flux $\Phi^{n+1,s}_{g,i-1/2,j}$ has the same form as (24), which can be written as

$$
\begin{aligned} \Phi^{n+1,s}_{g,i-1/2,j} &= A^{n+1,s}_{g,i-1/2,j}\sum_{m=1}^{M}\omega_m\mu_m(I^-_{i-1,j,m,g}1_{\mu_m>0} + I^+_{i,j,m,g}1_{\mu_m<0}) \\ &\quad + \frac{4\pi D^{n+1,s}_{g,i-1/2,j}}{3}\Big(\frac{\phi^{n+1,s+1}_{g,i,j} - \phi^{n+1,s+1}_{g,i-1,j}}{\Delta x}\Big) \\ &\quad + B^{n+1,s}_{g,i-1/2,j}\sum_{m=1}^{M}\omega_m\mu_m^2(\delta_x I^n_{i-1,j,m,g}1_{\mu_m>0} + \delta_x I^n_{i,j,m,g}1_{\mu_m<0}), \end{aligned}
$$

where we have replaced $I^{n+1}_{i,j,m,g}$ by $I^{n+1,l}_{i,j,m,g}$ and $I^{n+1}_{i-1,j,m,g}$ by $I^{n+1,l}_{i-1,j,m,g}$ in (18) to calculate $I^-_{i-1,j,m,g}$ and $I^+_{i,j,m,g}$ in the macro boundary flux $\Phi^{n+1,s}_{g,i-1/2,j}$.

3.3) For the system (30), use the Gauss-Seidel iteration to solve the resulting linear algebraic system.

3.4) Compute the relative iteration error. Stop the iteration when the convergent requirement is satisfied.

4) Update the solutions $\rho^{n+1}_{g,i,j} = \rho^{n+1,s+1}_{g,i,j}$ $(g = 1, \cdots, G)$ and $\tilde{T}^{n+1}_{i,j} = \tilde{T}^{n+1,s+1}_{i,j}$, and then the values of $\bar{\phi}^{n+1}_{g,i,j}$ $(g = 1, \cdots, G)$.

End

Source iteration algorithm for solving (28) and (29)

Based on the initial radiation intensity $I^n_{i,j,m,g}$ and $T^n_{i,j}$, $\tilde{T}^{n+1}_{i,j}$ and $\bar{\phi}^{n+1}_{g,i,j}(g = 1,\cdots,G)$ from the above mentioned iteration, find $I^{n+1,l}_{i,j,m,g}$ and $T^{n+1,l}_{i,j}$ for the approximations $I^{n+1}_{i,j,m,g}$ and $T^{n+1}_{i,j}$ in the equations(28) and (29).

1) Set the initial iterative value: $I^{n+1,l,0}_{i,j,m,g} = I^{n+1,l-1}_{i,j,m,g}$ and $T^{n+1,l,0}_{i,j} = T^{n+1,l-1}_{i,j}$;
2) Evaluate the boundary fluxes in (28), which implicitly depend on the unknowns $I^{n+1,l}_{i,j,m,g}$.
3) For $s = 1,\cdots,S$,

3.1) Calculate the predict material temperature $T^{n+1,*}_{i,j}$ from the equation (29) by

$$T^{n+1,*}_{i,j} = \frac{C_v T^n_{i,j} + \Delta t \sum\limits_{g=1}^{g=G}\sum\limits_{m=1}^{M} \omega_m \frac{(\sigma^a_g)^{n+1}_{i,j} I^{n+1,l,s-1}_{i,j,m,g} - (\sigma^e_g)^{n+1}_{i,j}(\bar{\phi}^{n+1}_{g,i,j} + \frac{\partial \bar{\phi}_{g,i,j}}{\partial T}\tilde{T}^{n+1}_{i,j})}{\epsilon^2}}{C_v + \Delta t \sum\limits_{g=1}^{g=G}\sum\limits_{m=1}^{M} \omega_m (\sigma^e_g)^{n+1}_{i,j} \frac{\partial \bar{\phi}_{g,i,j}}{\partial T}}.$$

3.2) Solve the source term $\tilde{\phi}_{g,i,j}$ of the equation (28) from (26) by

$$\tilde{\phi}_{g,i,j} = \bar{\phi}^{n+1}_{g,i,j} + \frac{\partial \bar{\phi}_{g,i,j}}{\partial T}(T^{n+1,*}_{i,j} - \tilde{T}^{n+1}_{i,j}).$$

3.3) Solve the implicit equation (28) by iteration.
3.4) Compute the relative source iteration error by

$$\text{error} = \Big| \sum_{g=1}^{g=G}\sum_{m=1}^{M} \omega_m (\sigma^a_g)^{n+1}_{i,j} I^{n+1,l,s}_{i,j,m,g} - \sum_{g=1}^{g=G}\sum_{m=1}^{M} \omega_m (\sigma^a_g)^{n+1}_{i,j} I^{n+1,l,s-1}_{i,j,m,g} \Big|.$$

Stop the iteration when the convergent requirement is satisfied.

4) With the help of the convergent value $I^{n+1,l,s}_{i,j,m,g}$, use (29) again to obtain the material temperature $T^{n+1,l}_{i,j}$ by

$$T^{n+1,l}_{i,j} = \frac{C_v T^n_{i,j} + \Delta t \sum\limits_{g=1}^{g=G}\sum\limits_{m=1}^{M} \omega_m \frac{(\sigma^a_g)^{n+1}_{i,j} I^{n+1,l,s}_{i,j,m,g} - (\sigma^e_g)^{n+1}_{i,j}(\bar{\phi}^{n+1}_{g,i,j} + \frac{\partial \bar{\phi}_{g,i,j}}{\partial T}\tilde{T}^{n+1}_{i,j})}{\epsilon^2}}{C_v + \Delta t \sum\limits_{g=1}^{g=G}\sum\limits_{m=1}^{M} \omega_m (\sigma^e_g)^{n+1}_{i,j} \frac{\partial \bar{\phi}_{g,i,j}}{\partial T}}. \tag{31}$$

4) Update the solutions $I^{n+1,l}_{i,j,m,g} = I^{n+1,l,s}_{i,j,m,g}$.

In order to make the algorithm more clearly, the flowchart for the computation procedures is given in Fig.1.

4. Asymptotic analysis of the current IUGKS

In this section we shall analyze the asymptotic property as $\epsilon \to 0$ of the current IUGKS. The techniques in [20, 22, 27] will be adapted for our analysis. From the asymptotic preserving analysis in [22, 27], the AP-property of the current IUGKS is mainly determined by the numerical fluxes, which are controlled through the ϵ-dependent coefficients in (20). These coefficient functions for the frequency-dependent system (1) possess the following properties.

Proposition 1. *Let the multi-group opacities σ^e_g and σ^a_g be positive. Then, as $\epsilon \to 0$, we have*

- *$A_g(\Delta t, \epsilon, \lambda_g)$ tends to 0;*

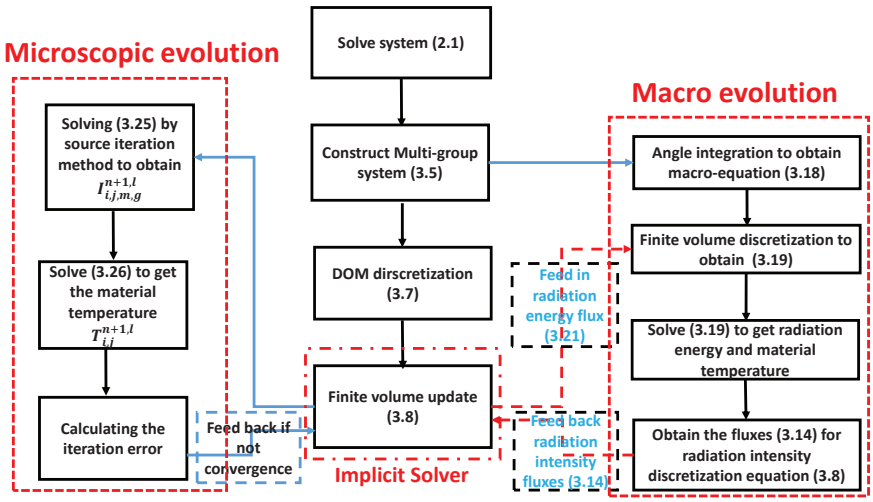

FIGURE 1. The flowchart of IUGKS.

- $B_g(\Delta t, \epsilon, \lambda_g)$ *tends to 0;*
- $D_g(\Delta t, \epsilon, \sigma_g^e, \lambda_g)$ *tends to* $-c\sigma_g^e/(\sigma_g^a)^2$.

Thus, the corresponding macroscopic diffusion flux $(\text{Diff})_{g,i-1/2,j}^{n+1}$, defined by

$$
\begin{aligned}
(\text{Diff})_{g,i-1/2,j}^{n+1} &= < \tfrac{c\mu}{\epsilon\Delta t} \int_{t^n}^{t^{n+1}} I_g(t, x_{i-1/2}, y_j, \mu, \xi) dt > \\
&= \int_{4\pi} \tfrac{c\mu}{\epsilon\Delta t} \int_{t^n}^{t^{n+1}} I_g(t, x_{i-1/2}, y_j, \mu, \xi) dt d\mu d\xi,
\end{aligned} \tag{32}
$$

has the limit

$$
\begin{aligned}
(\text{Diff})_{g,i-1/2,j}^{n+1} &= \textstyle\sum_{m=1}^{M} \omega_m \mu_m I_{m,g}(t, x_{i-1/2}, y_j, \mu_m, \xi_m) \\
\xrightarrow[\epsilon\to 0]{} & -4\pi \Big(\tfrac{c\sigma_{g,i-1/2,j}^e}{6(\sigma_{g,i-1/2,j}^a)^2} \delta_x \phi_{g,i-1/2,j}^{n+1,L} + \tfrac{c\sigma_{g,i-1/2,j}^e}{6(\sigma_{g,i-1/2,j}^a)^2} \delta_x \phi_{g,i-1/2,j}^{n+1,R} \Big) \\
&= -\tfrac{4\pi c\sigma_{g,i-1/2,j}^e}{3(\sigma_{g,i-1/2,j}^a)^2} \tfrac{\phi_{i,j}^{n+1} - \phi_{i-1,j}^{n+1}}{\Delta x}.
\end{aligned} \tag{33}
$$

The limiting function (33) gives a numerical flux, which exactly corresponds to the so-called standard three points scheme for the asymptotic diffusion equation in the one-dimensional case. It will become the five points scheme in the two-dimensional case. This shows that the current IUGKS is asymptotically preserving.

5. Numerical tests

This section presents a number of examples to validate the proposed AP-IUGKS for frequency-dependent radiative transfer equations. In the computations, the unit of length is taken to be centimeter (cm), mass unit is gramme (g), time unit is nanosecond (ns), temperature unit is kilo electronvolt (Kev), and energy unit is 10^9 Joules (GJ). Under the above units, the speed of light is $29.98 cm/ns$, and the radiation constant a is $0.01372\ GJ/cm^3 - keV^4$. In order to compare with the results computed by the explicit UGKS from [27], we first define the explicit time step by $\Delta t = CFL * \min\{\Delta x, \Delta y\} * \epsilon/c$, where Δx and Δy are the minimal spatial

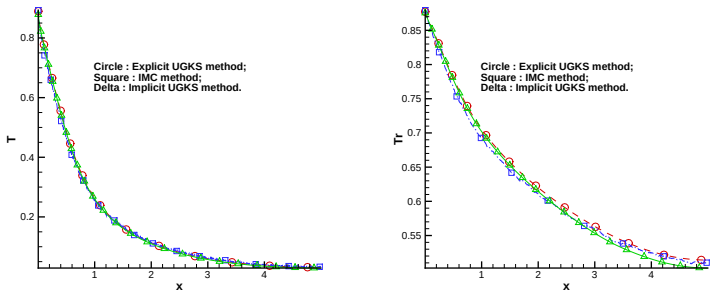

FIGURE 2. Results at $1ns$ for case one of example one with homogeneous opacity $\sigma_0 = 10keV^{7/2}/cm$.

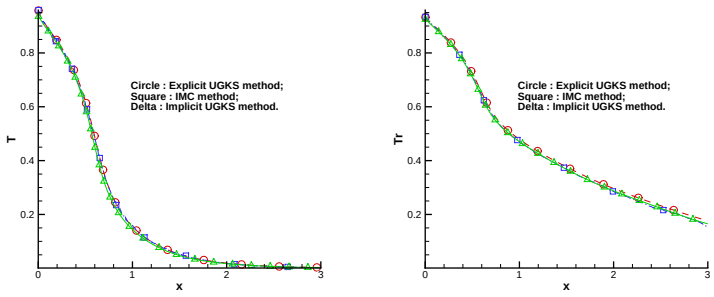

FIGURE 3. Results at $1ns$ for case one of example one with homogeneous opacity $\sigma_0 = 100keV^{7/2}/cm$.

mesh steps in x-direction and y-direction, respectively. The Courant number CFL takes a value 0.8 in the following numerical tests for the UGKS method in [22, 27]. For the IUGKS simulations, we introduce the time-step enlarging factor $f_e = 1.2$ and shortening factor $f_s = 0.8$. Then, the implicit time step can be enlarged or shortened with the factor f_e or f_s based on the iteration numbers s of source iteration algorithm in the last step.

In the following tests the opacity for both IUGKS and UGKS uses the simple group integration averaging, and the implicit Monte Carlo method (IMC) uses the point value. In order to compare the computational times of IUGKS, UGKS and IMC, both codes are running in ThinkPad X250 (Intel(R) Core(TM) i7-5600U).

Example 1. (see [6]) In this example, we consider a one-dimension Cartesian coordinate with a constant heat capacity $C_v = 0.1GJ/keV/cm^3$ and an opacity of the form

$$\sigma(x, \nu, T) = \frac{\sigma_0(x)}{(h\nu)^3\sqrt{kT}}.$$

The initial material temperature is 10^{-3} keV, and the initial radiation intensity is given by a Planck distribution evaluated at the same temperature. The incident radiation intensity on the left boundary is also given by a Planck distribution, but associated with a temperature of 1keV. A reflective boundary condition is used on the right boundary. This test will cover three cases with different optical opacity

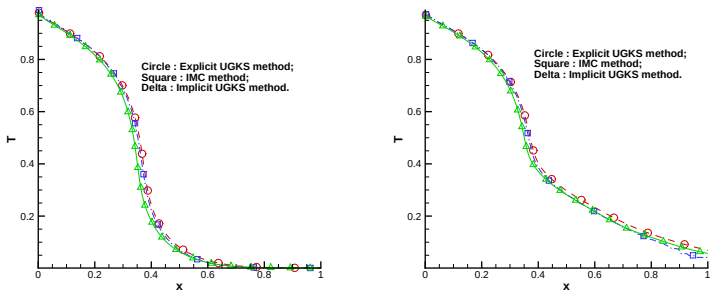

FIGURE 4. Results at $1ns$ for case one of example one with homogeneous opacity $\sigma_0 = 1000keV^{7/2}/cm$.

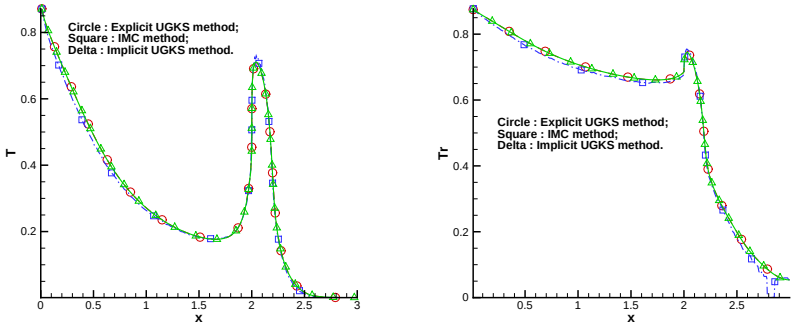

FIGURE 5. Results at $1ns$ for case two of example one with the first heterogeneous opacities and with local mesh refinement.

specified by σ_0. To represent the frequency dependent opacity, UGKS employs 30 frequency groups spaced logarithmically between $10^{-4}keV$ and $100keV$. The multi-group opacities are evaluated simply by averaging it over each group.

Case one: Several homogeneous problems are tested in a domain of $5cm$ thickness with $\sigma_0 = 10keV^{7/2}/cm$, $100keV^{7/2}/cm$, and $1000keV^{7/2}/cm$. In all three cases, a uniform spatial mesh is used with cell size $\Delta x = 0.005cm$ and a running time of $1ns$. Figs. 2–4 present the material and radiation temperatures computed by IUGKS, UGKS and IMC. Note that in Figs. 3 and 4 only the portions with large material temperature variation are shown. The material temperature computed by IUGKS agrees well with that by UGKS and IMC.

Case two: In this case, we consider the first heterogeneous problem, which covers a domain of $3cm$ thickness divided by an optically thin region $0cm < x < 2cm$ and an optically thick region $2cm < x < 3cm$, where σ_0 is defined by

$$\sigma_0(x) = \begin{cases} 10keV^{7/2}/cm, & 0cm < x < 2cm, \\ 1000keV^{7/2}/cm, & 2cm < x < 3cm. \end{cases}$$

In the computation, the cell size is $\Delta x = 0.02cm$ in the optically thin region and $\Delta x = 0.005cm$ in the optically thick region. Furthermore, in order to resolve the opacity thin and thick interface, we divided the leftmost cell in the optically thick region into 10 smaller cells, where the size of each cell increased by a factor of

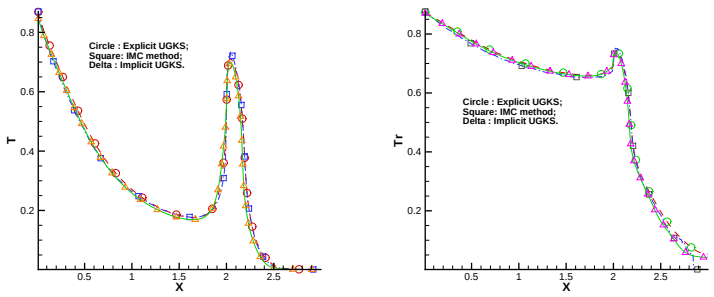

FIGURE 6. Results at $1ns$ for case two of example one with the first heterogeneous opacities and without local mesh refinement.

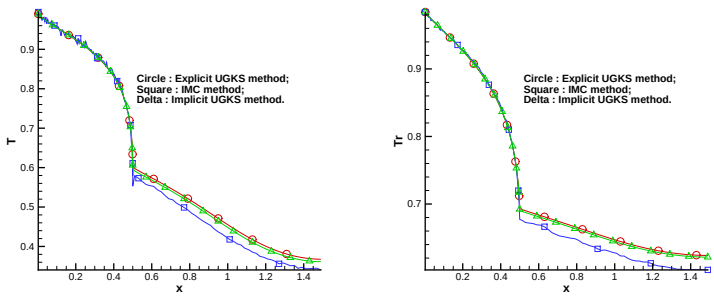

FIGURE 7. Results at $5ns$ for case three of example one with the second heterogeneous opacities and with local mesh refinement.

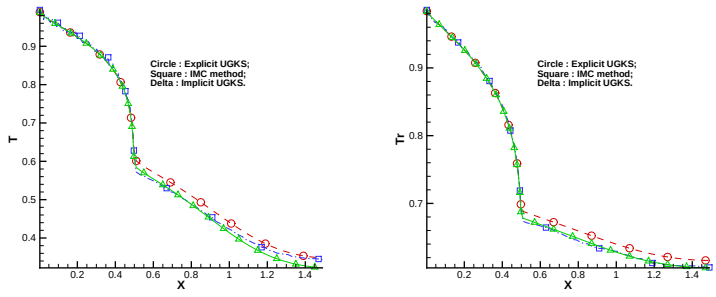

FIGURE 8. Results at $5ns$ for case three of example one with the second heterogeneous opacities and without local mesh refinement.

1.47394 from left to right. The simulation runs up to the time of $1ns$. Fig. 5 shows the computed results by UGKS, IUGKS and IMC with local mesh refinement, and Fig. 6 without local mesh refinement where it is clear to see that good agreement in the simulation results with/without local mesh refinement has been obtained.

Case three: In this case, we consider the second heterogeneous problem in a domain of $1.5cm$ thickness, but with reversed locations for the optically thin and thick regions. Specifically, this domain is composed of an optically thick region in

TABLE 1. The computation time of UGKS and IMC for Example one.

Example one		UGKS	IMC	IUGKS
case one	$\sigma_0 = 10$	65 minutes	96 minutes	35 minutes
	$\sigma_0 = 100$	69 minutes	173 minutes	34 minutes
	$\sigma_0 = 1000$	86 minutes	1344 minutes	67 minutes
case two	refinement	617 minutes	735 minutes	430 minutes
	No Refinement	17 minutes	363 minutes	12 minutes
case two	heterogeneous with mesh refinement	617 minutes	363 minutes	430 minutes
case three	refinement	1799 minutes	6279 minutes	739 minutes
	No Refinement	44 minutes	5184 minutes	40 minutes

$0cm < x < 0.5cm$ and an optically thin region in $0.5cm < x < 1.5cm$ with σ_0 given by

$$\sigma_0(x) = \begin{cases} 1000keV^{7/2}/cm, & 0cm < x < 0.5cm, \\ 10keV^{7/2}/cm, & 0.5cm < x < 1.5cm. \end{cases}$$

A spatial mesh with cell size $\Delta x = 0.02cm$ in the optically thin region and $\Delta x = 0.005cm$ in the optically thick region is used. And furthermore, in order to resolve the opacity thin and thick interface, we divided the rightmost cell in the optically thick region into 10 smaller cells, where the size of each cell is decreased by a factor of 0.678455 from left to right. The simulation runs up to a time of $5ns$. Fig. 7 presents the UGKS, IUGKS and IMC solutions with local mesh refinement, and Fig. 8 without local mesh refinement. There are slight differences between these two solutions in the optical thin region.

The computational times of UGKS, IUGKS and IMC for all three cases are shown in Table 1. In general, IUGKS is much more efficient than UGKS and IMC with the same spatial mesh size, in particular, for the optical thick case.

Remark : The computational time in Table 1 of this paper for UGKS is longer than that in [27]. This is just due to the different choice of the first iteration values for the linear algebraic equation solver in the algorithm of solving (22). In [27] we use the initial values as the first iteration values in every iteration step in the solution of the linear equation; and since the time step is small, this will not damage the convergence. On the other hand, however, for IUGKS the time step is large, the choice in [27] can not give a proper solution in IUGKS. So, for IUGKS we choose here the last nonlinear iteration final values as the first iteration value for the next iteration step. In order to compare the computational time, we take a first iteration value for UGKS similar to that for IUGKS in this paper.

Example 2. (Larsen's Test Problem [3, 15]) For this problem, the frequency variable ν is logarithmaically spaced with 50 groups between $h\nu_{min} = 10^{-5}keV$ and $h\nu_{max} = 10keV$. Group g is defined by $\nu_{g-\frac{1}{2}} \le \nu \le \nu_{g+\frac{1}{2}}$, where

$$\nu_{\frac{1}{2}} = \nu_{min}, \qquad \nu_{g+\frac{1}{2}} = (\frac{\nu_{max}}{\nu_{min}})^{\frac{1}{50}} \nu_{g-\frac{1}{2}}.$$

The computational domain is divided into three regions with different cell size,

$$\Delta x = \begin{cases} 0.10cm, & 0cm < x < 1cm, \\ 0.02cm, & 1cm < x < 2cm, \\ 0.20cm, & 2cm < x < 4cm. \end{cases}$$

The opacity models photo-ionization absorption,

$$\sigma(\nu, T, x) = \gamma(x) \frac{1 - e^{-h\nu/kT}}{(h\nu)^3},$$

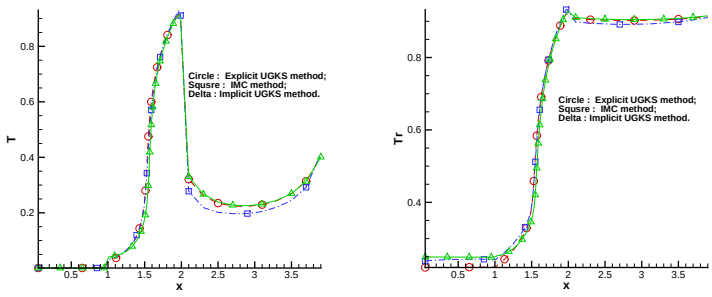

FIGURE 9. Results of Larsen's tests (example two) at $900ps$.

TABLE 2. The computation time of UGKS and IMC for Example two.

UGKS	IMC	IUGKS
2 minutes	63 minutes	1 minutes

where

$$\gamma(x) = \begin{cases} 1keV^3/cm, & 0cm < x < 1cm, \\ 1000keV^3/cm, & 1cm < x < 2cm, \\ 1keV^3/cm, & 2cm < x < 4cm. \end{cases}$$

The heat capacity C_v keeps a constant value $5.109 \times 10^{14} erg \cdot keV^{-1} cm^{-3}$. The initial material temperature is given by $T(x,0) = 10^{-3} keV$, which is in equilibrium with the initial radiation intensity. No radiation enters from the left boundary, but a steady, direction-dependent, $1keV$ Planckian distribution of photons enters from the right boundary. The simulation runs up to a time of $900ps$. Fig. 9 shows good agreement in the IUGKS, UGKS and IMC solutions in the middle opacity thick region. But small differences appear among the solutions in the opacity thin regions. The computational costs of IUGKS, UGKS and IMC for this case are given in Table 2, from which it is clear to see that IUGKS is the most efficient.

6. Conclusion

By employing a back-time approximation to construct the implicitly (in time) radiation-intensity-dependent boundary fluxes, we have proposed an asymptotic preserving implicit unified gas kinetic scheme (IUGKS) for the frequency-dependent radiative transfer system. Compared with the explicit unified gas kinetic scheme (UGKS) given in [27] where the time step should be constrained by the CFL condition and could be very small in small spatial mesh regions, larger time steps can be used in small spatial meshes for IUGKS, and computational costs can be saved therefore. Moreover, in contrast to UGKS, it is shown here that the asymptotic preserving property of IUGKS holds uniformly with respect to the small Knudsen number. We have presented a number of numerical tests and compared the numerical results by IUGKS with those computed by UGKS and IMC. The numerical results show that IUGKS is computationally cheap in comparison with UGKS and IMC, and the computational efficiency can be improved greatly.

Acknowledgments

The authors wish to thank the referees for the useful suggestions which improve this paper. The current research was supported by NSFC (Grant No. 11671048, 91630310, 11371068) and the Science and Technology Development foundation of China Academy of Engineering Physics(Grant No.2015B0202041, 2015B0202040) for Sun; by the National Basic Research Program under Grant 2014CB745002 and NSFC (Grant Nos. 11229101, 11631008, 11371065) for Jiang; by Hong Kong research grant council (620813,16211014), HKUST SBI14SC11, and NSFC-91330203 for Xu. The authors would like to thank Professor Shu Li at Institute of Applied Physics and Computational Mathematics for providing the IMC results.

References

[1] M.L. Adams, NUEN 630: Computational Methods for Particle-Transport Problems, Class Notes, Texas *A&M* University (2004).
[2] M.L. Admas and P.F. Nowak, Asymptotic Analysis of a Computational Method for Time- and Frequency-Dependent Radiative Transfer. J. Comput. Phys. 146 (1998), pp. 366-403.
[3] B. Chang, The incorporation of the semi-implicit linear equations into Newton's method to solve radiation transfer equations. J. Comput. Phys., 226 (2007), pp. 852-878.
[4] S.Z. Chen, K. Xu, C.B. Lee, and Q.D. Cai, A unified gas kinetic scheme with moving mesh and velocity space adaptation, J. Comput. Phys. 231 (2012), pp. 6643-6664.
[5] S.Z. Chen and K. Xu, A comparative study of an asymptotic preserving scheme and unified gas-kinetic scheme in continuum flow limit, J. Comput. Phys. 288 (2015), pp. 52-65.
[6] J.D. Densmore, K.G. Thompson and T.J. Urbatsch, A hybrid transport-diffusion Monte Carlo method for frequency-dependent radiative-transfer simulations. J. Comput. Phys. 231 (2012), pp. 6924-6934.
[7] N.A. Gentile, Implicit Monte Carlo diffusion - an accerlation method for Monte Carlo time-dependent radiative transfer simulations. J. Comput. Phys. 172 (2001), pp. 543-571.
[8] J.R. Howell, R. Siegel, M.P. Menguc, Thermal Radiation Heat Transfer, Fifth Edition, Taylor & Francis (2011).
[9] J.C. Huang, K. Xu, and P.B. Yu, A unified gas-kinetic scheme for continuum and rarefied flows II: multi-dimensional cases, Communications in Computational Physics 12 (2012), pp. 662-690.
[10] S. Jin and C.D. Levermore, The discrete-ordinate method in diffusive regimes, Transport Theory Statist. Phys. 20 (1991), pp. 413-439.
[11] S. Jin and C.D. Levermore, Fully discrete numerical transfer in diffusive regimes, Transport Theory Statist. Phys. 22 (1993), pp. 739-791.
[12] S. Jin, L. Pareschi and G. Toscani, Uniformly accurate diffusive relaxation schemes for multiscale transport equations, SIAM J. Numer. Anal. 38 (2000), pp. 913-936.
[13] A. Klar, An asymptotic-induced scheme for nonstationary transport equations in the diffusive limit, SIAM J. Numer. Anal. 35 (1998), pp. 1073-1094.
[14] A. Klar, C. Schmeiser, Numerical passage from radiative transfer to nonlinear diffusion models, Math. Meth. Mod. Appl. Sci. 11 (2001), pp. 749-767.
[15] E.W. Larsen, A grey transport acceleration method for time-dependent radiative transfer problems. J. Comput. Phys. 78 (1988), pp. 459-480.
[16] A.W. Larsen and J.E. Morel, Asymptotic solutions of numerical transport problems in optically thick, diffusive regimes. II, J. Comp. Phys. 83 (1989), pp. 212-236.
[17] A.W. Larsen, J.E. Morel and W.F. Miller Jr., Asymptotic solutions of numerical transport problems in optically thick, diffusiive regimes. J. Comput. Phys. 69 (1987), pp. 283-324.
[18] E.W. Larsen, G.C.Pomraning and V.C.Badham, Asymptotic analysis of radiative transfer problems, J. Quant. Spectrosc. Radiat. Transfer 29 (1983), pp. 285.
[19] C.E. Lee, The Discrete S_N Approximation to Transport Theory, LA-2595 (1962).
[20] L. Mieussens, On the asymptotic preserving property of the unified gas kinetic scheme for the diffusion limit of linear kinetic model. J. Comput. Phys. 253 (2013), pp. 138-156.
[21] M.F. Modest, Radiative Heat Transfer, Third Edition, Academic Press (2013).
[22] W.J. Sun, S. Jiang, and K. Xu, An Asymptotic Preserving unified gas kinetic scheme for gray radiative transfer equations. J. Comput. Phys. 285 (2015), pp. 265-279.

[23] B. van Leer, Towards the ultimate conservative difference schemes V. A second-order sequal to Godunov's method. J. Comput. Phys. 32 (1979), pp. 101-136.
[24] K. Xu, Direct modeling for computational fluid dynamics: construction and application of unfied gas kinetic schemes, World Scientific (2015).
[25] K. Xu, Direct modeling for computational fluid dynamics, Acta Mech Sin 31 (2015), pp. 303-318.
[26] K. Xu and J.C. Huang, A unified gas-kinetic scheme for continuum and rarefied flows. J. Comput. Phys. 229 (2010), pp. 7747-7764.
[27] W.J. Sun, S. Jiang, K. Xu and S. Li, An asymptotic preserving unified gas kinetic scheme for frequency-dependent radiative transfer equations. J. Comput. Phys. 302 (2015), pp. 222-238.

Institute of Applied Physics and Computational Mathematics, P.O. Box 8009, Beijing 100088, China
E-mail: sun_wenjun@iapcm.ac.cn, jiang@iapcm.ac.cn

Department of Mathematics and Department of Mechanical and Aerospace Engineering, Hong Kong University of Science and Technology, Hong Kong, China
E-mail: makxu@ust.hk